Brief Communication

MOLECULAR METABOLISM

A reduced form of nicotinamide riboside defines a new path for NAD^+ biosynthesis and acts as an orally bioavailable NAD^+ precursor

Judith Giroud-Gerbetant [1,5], Magali Joffraud [1,5], Maria Pilar Giner [1], Angelique Cercillieux [1,2], Simona Bartova [1], Mikhail V. Makarov [3], Rubén Zapata-Pérez [4], José L. Sánchez-García [1], Riekelt H. Houtkooper [4], Marie E. Migaud [3], Sofia Moco [1], Carles Canto [1,2,*]

ABSTRACT

Objective: A decay in intracellular NAD^+ levels is one of the hallmarks of physiological decline in normal tissue functions. Accordingly, dietary supplementation with NAD^+ precursors can prevent, alleviate, or even reverse multiple metabolic complications and age-related disorders in diverse model organisms. Within the constellation of NAD^+ precursors, nicotinamide riboside (NR) has gained attention due to its potent NAD^+ biosynthetic effects *in vivo* while lacking adverse clinical effects. Nevertheless, NR is not stable in circulation, and its utilization is rate-limited by the expression of nicotinamide riboside kinases (NRKs). Therefore, there is a strong interest in identifying new effective NAD^+ precursors that can overcome these limitations.

Methods: Through a combination of metabolomics and pharmacological approaches, we describe how NRH, a reduced form of NR, serves as a potent NAD^+ precursor in mammalian cells and mice.

Results: NRH acts as a more potent and faster NAD^+ precursor than NR in mammalian cells and tissues. Despite the minor structural difference, we found that NRH uses different steps and enzymes to synthesize NAD^+, thus revealing a new NRK1-independent pathway for NAD^+ synthesis. Finally, we provide evidence that NRH is orally bioavailable in mice and prevents cisplatin-induced acute kidney injury.

Conclusions: Our data identify a new pathway for NAD^+ synthesis and classify NRH as a promising new therapeutic strategy to enhance NAD^+ levels.

Keywords NAD^+; Nicotinamide riboside; Metabolism

1. INTRODUCTION

Over 100 years ago, nicotinamide adenine dinucleotide (NAD^+) was discovered, first as a coenzyme and later as an essential cofactor in cellular redox reactions to produce energy [1]. NAD^+ plays critical roles in energy metabolism, as the oxidation of NADH to NAD^+ enables hydride transfer and subsequent ATP generation through mitochondrial oxidative phosphorylation [1]. NAD^+ also acts as a degradation substrate for multiple enzymes such as the sirtuin family of protein deacylases [2], poly (ADP-ribose) polymerases [3], and ADP-ribose cyclases [4].

Mammalian organisms can synthesize NAD^+ from different sources [1]. First, NAD^+ can be obtained from tryptophan through the 10-step *de novo* pathway. Nicotinic acid (NA) can also be transformed into NAD^+ through the 3-step Preiss-Handler pathway, which converges with the *de novo* pathway. The intracellular NAD^+ salvage pathway from nicotinamide (NAM) constitutes the main path by which cells build NAD^+ [1] and progresses through a 2-step reaction in which NAM is first transformed into NAM-mononucleotide (NMN) via the catalytic activity of NAM-phosphoribosyltransferase (NAMPT) and is then converted to NAD^+ via NMN adenylyltransferase (NMNAT) enzymes. Bieganowski and Brenner described how nicotinamide riboside (NR) constitutes yet a fourth path to NAD^+, characterized by the initial phosphorylation of NR into NMN by NR kinases (NRKs) [5].

NA and NAM, collectively termed niacin, were used previously to treat pellagra, which is an overt state of NAD^+ deficiency and dyslipidemia [6]. However, NA acts as an agonist of the G-protein-coupled receptor Gpr109A, even at subtherapeutic doses, leading to a painful, spontaneous flushing response [7–10]. NAM, as a stand-alone agent, lacks therapeutic effectiveness as a lipid-lowering agent or against

[1]Nestlé Institute of Health Sciences, Nestlé Research, EPFL Innovation Park, 1015, Lausanne, Switzerland [2]School of Life Sciences, EPFL, Lausanne, 1015, Switzerland [3]Mitchell Cancer Institute, University of South Alabama, 1660 Springhill Avenue, Mobile, 36604, Alabama, USA [4]Laboratory Genetic Metabolic Diseases, Amsterdam Gastroenterology and Metabolism, Amsterdam Cardiovascular Sciences, Amsterdam UMC, University of Amsterdam, Meibergdreef 9, Amsterdam, the Netherlands

[5] Judith Giroud-Gerbetant and Magali Joffraud contributed equally to this work.

*Corresponding author. Nestlé Institute of Health Sciences, Nestlé Research EPFL campus, Quartier de l'Innovation, Bâtiment G, Lausanne, CH-1015, Switzerland. E-mail: carlos.cantoalvarez@rd.nestle.com (C. Canto).

Received June 5, 2019 • Revision received September 13, 2019 • Accepted September 28, 2019 • Available online 3 October 2019

https://doi.org/10.1016/j.molmet.2019.09.013

metabolic complications, which could be partially attributed to the fact that it acts as an end-product inhibitor of NAD^+-consuming enzymes [6]. This has driven considerable attention to the use of NR or even NMN as dietary supplements. Administration of either compound in rodents has been shown to reduce diet- and age-related metabolic complications, including insulin sensitivity [11–13], fatty liver [13,14], and kidney damage [15]. Similarly, both compounds afforded protection against age-related physiological decline in mice [16,17]. NR, in particular, has been shown to increase the lifespan of all species tested to date, including mice [17–19]. The very similar actions of both compounds might be explained by data indicating that NMN needs to be extracellularly converted to NR to be taken up by the cells [20,21]. Recent clinical studies revealed that NR has an excellent safety profile up to 2 g per day [22–24]; however, thus far, only mild benefits on blood pressure [24] and exercise performance in elderly individuals [25] have been identified. The actions of oral NR intake, however, might be constrained by several factors, one being that NR rapidly degrades to NAM in plasma [20]. Accordingly, NAM levels in plasma, as well as those of NAM methylation and oxidation products, increase shortly after NR administration [18,22]. In addition, recent evidence suggests that the degradation of NR could compromise the ability of the compound to reach peripheral tissues after oral intake [26]. In this study, we aimed to explore whether a small modification of the NR molecule could prevent its degradation. Through this premise, we identified NRH, a reduced form of NR, as a new NAD^+ precursor. NRH shows an unprecedented ability to increase NAD^+ in cultured cells and mice, as it is more potent and faster than NR. Despite the minor chemical modification, NRH utilizes a different path than NR to synthesize NAD^+, which is NRK independent. We also demonstrate that NRH is protected against degradation in the plasma and can be detected in circulation after oral administration. Finally, NRH also demonstrates therapeutic efficacy against cisplatin-induced kidney injury. Overall, in this work, we identify NRH as a new potential molecule for NAD^+-based therapies and reveal a novel path for NAD^+ synthesis.

2. MATERIALS AND METHODS

2.1. NRH synthesis

1-[(2R,3R,4S,5R)-3,4-Dihydroxy-5-(hydroxymethyl)tetrahydrofuran-2-yl]-4H-pyridine-3-carboxamide (NRH) was generated from triacetylated NR triflate by reduction with sodium dithionite, followed by methanolic deprotection of all the acetate groups. ^1H and ^{13}C NMR spectral and MS spectrometry data of NRH were as follows: ^1H NMR (D_2O, 400 MHz), δ, ppm: 2.98 (q, 2H, J = 1.5 Hz, H4), 3.26 (s, 1.5H, 0.5 MeOH), 3.60 and 3.66 (AB part of the ABX system, 2H, J_{AB} = 12.5 Hz, J_{BX} = 4.8 Hz, J_{AX} = 3.6 Hz, H5′$_A$, H5′$_B$), 3.88 (dd, 1H, J = 6.8 Hz, J = 3.5 Hz, H4′), 4.04 (dd, 1H, J = 2.9 Hz, $^3J_{HH}$=5.6 Hz, H3′), 4.11 (m, 1H, H2′), 4.66 (OH, NH_2 overlapped with D_2O), 4.79 (d, 1H, J = 7.0 Hz, H1′), 4.90 (dt, 1H, J = 8.2 Hz, J = 3.8 Hz, H5), 6.01 (dd, 1H, J = 1.5 Hz, J = 8.2 Hz, H6), and 7.06 (s, 1H, H2). ^{13}C NMR (D_2O, 100 MHz), δ, ppm: 22.07 (C4), 49.00 (MeOH), 61.63 (C5′), 70.21 (C3′), 71.11 (C2′), 83.56 (C4′), 95.03 (C1′), 101.08 (C3), 105.20 (C5), 125.37 (C6), 137.80 (C2), and 172.96 (CO). MS (ESI): m/z = 257.21 (M + 1). HRMS found: 257.11376. Calculated for $C_{11}H_{17}N_2O_5$ (M+1): 257.113198.

2.2. Cell culture

Unless otherwise specified, all the common cell culture media and reagents were obtained from Gibco (Thermo Fisher Scientific). AML12 cells were cultured in Dulbecco's modified Eagle's medium/nutrient mixture F-12 (DMEM:F-12), supplemented with 10% FBS, 1x insulin/transferrin/selenium solution from Gibco (ITS-G), and 100 nM dexamethasone. To evaluate the ability of the compounds to stimulate NAD^+ synthesis, the cells were treated with PBS (as vehicle), NR, or NRH at the concentrations indicated.

INS1E cells were seeded in 6-well plates at a concentration of 0.8 million cells per well and then left for 24 h in growth media (RPMI 1640 complemented with 10% FBS, 1% penicillin-streptomycin (P/S), 10 mM HEPES, 1 mM sodium pyruvate, and 0.05 mM β-mercaptoethanol. The cells were then washed once with PBS and treated with either PBS (as a vehicle) or 0.5 mM NRH. The cells were then trypsinized and collected for NAD^+ and protein content measurements.

C2C12 cells were seeded in 6-well plates at a concentration of 0.5 million cells per well and grown in DMEM media containing 20% FBS, 1% P/S, 10 mM HEPES, and 2 mM sodium pyruvate. Once the cells were 80% confluent, they were differentiated for 6 days by adding them to a similar DMEM media containing 2% horse serum instead of 20% FBS. The cells were then treated with PBS (as a vehicle) or NRH (0.5 mM), trypsinized and used for NAD^+ and protein measurements.

3T3/NIH fibroblasts were cultured in DMEM supplemented with 10% FBS, 1% P/S, 10 mM HEPES, and 1 mM sodium pyruvate and treated with PBS (as a vehicle) or NRH (0.5 mM) as described for the other cell types.

All the cells used in this study were verified as mycoplasma-free using a MycoProbe Mycoplasma Detection Kit (R&D cat. CUL001B). The chemical inhibitors used for the cell cultures were as follows: S-(4-nitrobenzyl)-6-thioinosine (NBTI; 10 μM; from Sigma–Aldrich, Ref: N2255), (E)-N-[4-(1-benzoylpiperidin-4-yl)butyl]-3-(pyridin-3-yl)acrylamide (FK866; 2 μM; from Sigma–Aldrich, Ref: F8557), 5-iodotubercidin (5-IT; 1 μM; from Tocris Bioscience, Ref: 1745), 5-(3-bromophenyl)-7-[6-(4-morpholinyl)-3-pyrido [2,3-d]byrimidin-4-amine dihydrochloride (ABT-702; 10 μM; from Tocris Bioscience, Ref: 2372), and gallotannin (100 μM; from Sigma–Aldrich, Ref: 403040). DMSO (1:1000) was used for the respective control groups. The concentrations were based on previous publications ([21] for NBTI and FK866 and [27] for gallotannin) or the manufacturer's instructions and were used 1 h prior to treatment with NRH or PBS as vehicle.

2.3. In vivo experiments

All the animal experiments were performed according to national Swiss and EU ethical guidelines and approved by the local animal experimentation committee under license VD 2770. NRK1 KO mice were described previously [20]. All the mice had pure C57Bl/6NTac backgrounds. The mice were kept in a temperature- and humidity-controlled environment with a 12:12-h light-dark cycle. The mice had access to nesting materials and *ad libitum* access to water and a commercial low-fat diet (D12450J, Research Diets Inc.).

Primary hepatocytes were isolated from wild-type (WT) and NRK1 KO mice by continuous recirculating perfusion of the mouse liver *in situ* with collagenase digestion. Briefly, the perfusion was performed with Krebs buffer (4.7 mM KCl, 0.7 mM KH_2PO_5, 10 mM HEPES, 117 mM NaCl, 24.6 mM $NaHCO_3$, and 0.2% glucose) supplemented with 5 mM $CaCl_2$ and 0.5 mg/ml collagenase (Worthington, type IV) for 10 min with 5 ml/min flow. The cells were seeded in M199 containing 100 U/ml penicillin G, 100 μg/ml streptomycin, 0.1% (w/v) BSA, 10% (v/v) FBS, 10 nM insulin, 200 nM triiodothyronine, and 100 nM dexamethasone. Post-attachment (4–5 h), the cells were cultured overnight in M199 supplemented with antibiotics and 100 nM dexamethasone and used for experiments the following morning.

For the intraperitoneal injection and oral gavage experiments, the mice were fasted for 2 h and then intraperitoneally injected or orally gavaged with either saline, NR, or NRH at the concentrations indicated in the figure legends. Then, 1 h later, the mice were anesthetized using

isoflurane. Their blood was collected through intracardiac puncture, and their tissues were snap frozen in liquid nitrogen. The blood samples were immediately transferred to EDTA blood collection tubes, which were kept on ice. The samples were then centrifuged at 4 °C and 3000 rpm for 10 min in a temperature-controlled tabletop centrifuge to isolate the plasma.

For the acute kidney injury (AKI) study, we based our intervention on a well-standardized method for cisplatin-induced AKI in mice [28]. Briefly, 8-week-old mice were randomized into 4 experimental groups as described in the article. They were injected with either vehicle (saline) or cisplatin (20 mg/kg) simultaneously with either PBS or NRH (250 mg/kg). At 24, 48, and 72 h after the initiation of the experiment, the mice were again injected with either PBS or NRH. Then, 4 h after the last injection, the mice were anesthetized, their blood was collected by intracardiac puncture, and their kidney tissue was collected for the diverse analyses described in the study.

2.4. NAD^+ measurements

NAD^+ was extracted from both the tissue and cell cultures and quantified using an EnzyChrom NAD/NADH Assay Kit (BioAssay Systems) according to the manufacturer's instructions.

2.5. NAD^+ metabolomics

Biological samples (AML12 cells, 500 k—1000 k cells; plasma, 60 μL; kidney, ∼2—10 mg) were extracted in 1300 μL of a cold mixture of methanol:water:chloroform at 5:3:5 (v/v) with 5 μM NAM-D_4 and 60 μL [U]-^{13}C-NAD^+ labeled biomass from homemade yeast as internal standards while keeping the samples cold throughout the procedure. Kidney extracts were homogenized with 3 mm tungsten carbide beads using a tissue grinder (Qiagen TissueLyser II) for 3 min at 20 Hz. The AML12 cells were scraped from each well with a 1 mL pipette tip and transferred into tubes. All the samples were agitated for 10 min at 4 °C in a thermo-shaker (Thermomixer C, Eppendorf), followed by 10 min of centrifugation at 4 °C. The samples showed two phases, with the upper phase containing polar metabolites separated from the lower phase by a protein layer. This protein layer was used for quantification (kidney and AML12 cells) with a bicinchoninic acid (BCA) assay (Thermo Fisher Scientific). The upper polar phase was dried overnight in a vacuum centrifuge at 4 °C and 5 mbar and then stored at −80 °C before analysis. The dried samples were reconstituted in either 40 μL (AML12 cells) or 60 μL (kidney and plasma) in 60% (v/v) acetonitrile/water, and the supernatants transferred into glass vials for hydrophilic interaction ultra-high performance liquid chromatography mass spectrometry (UHPLC-MS) analysis. The UHPLC consisted of a binary pump, a cooled autosampler, and a column oven (DIONEX Ultimate 3000 UHPLC + Focused, Thermo Fisher Scientific) connected to a triple-quadrupole spectrometer (TSQ Vantage, Thermo Fisher Scientific) equipped with a heated electrospray ionization (H-ESI) source. For each sample, 2 μL were injected into the analytical column (2.1 mm × 150 mm, 5 μm pore size, 200 Å HILICON iHILIC-Fusion(P)) guarded by a pre-column (2.1 mm × 20 mm, 200 Å HILICON iHILIC-Fusion(P) Guard Kit) operating at 35 °C. The mobile phase (10 mM ammonium acetate at pH 9, A, and acetonitrile, B) was pumped at a 0.25 mL/min flow rate over a linear gradient of decreasing organic solvent (0.5—16 min, 90-25% B), followed by re-equilibration for a total run time of 30 min. The MS was operated in positive mode at 3500 V with multiple reaction monitoring (MRM), and in each scan event, the scan width was 1 *m/z*, the scan time was 0.05 s, and the peak width for Q1 was 0.25 FWHM and for Q3 was 0.70 FWHM. The sheath gas was 20 arbitrary units, and the auxiliary gas was kept at 15 arbitrary units. The vaporizer temperature was 280 °C and the ion transfer tube temperature was 310 °C. The tube lens voltage and collision energy were individually optimized for each fragment ion of NAD^+-related metabolites. Xcalibur software v4.1.31.9 (Thermo Fisher Scientific) was used for the instrument control and data acquisition and processing. Positive ion mode-extracted chromatograms using the MRM trace of NAM, 1-methyl-NAM (Me-NAM), NR, NRH, NMN, the reduced form of NMN (NMNH), nicotinic acid adenine dinucleotide (NAAD), nicotinic acid mononucleotide (NaMN), NAD^+, and NADH were integrated and used for relative comparison normalized to the internal standard (plasma, AML12 cells, and kidney) and total protein (AML12 cells and kidney). The retention time and mass detection of the metabolites were confirmed by authentic standards. NRH quantification in the plasma was performed using a calibration curve, including internal standard normalization. All the samples were randomized before the analysis of the experimental batches.

2.6. Protein and mRNA analysis

Total mRNAs were extracted, processed, and quantified as described previously [20]. The primers used are provided in Supplementary Table 1. Gene expression was normalized with β2-microglobulin and cyclophilin. Protein extraction and quantification, and western blotting procedures were performed as described previously [20] by adding 10 μM PJ-34 hydrochloride (Sigma—Aldrich, Ref: P4365) to the protein extraction buffer. The addition of PJ-34 was critical to visualize the high-molecular-weight smear of PARylated proteins in our samples. Poly (ADP-ribose) antibody was obtained from Enzo Life Sciences Inc. (Ref: ALX-210-890) and used at a 1:1000 dilution. PARP1 antibody was obtained from Cell Signaling Technology (Ref: 9532) and used at a 1:1000 dilution. Tubulin antibody was obtained from Sigma—Aldrich (Ref: T2096) and used at a 1:1000 dilution. Western blotting bands were quantified using ImageJ software.

2.7. Histology analyses

Kidney tissue samples were embedded in optimal cutting temperature compound (OCT) and then further stained for hematoxylin and eosin (H&E) or against anti-cleaved caspase-3 (Cell Signaling Technology; Ref: 9661). All the staining procedures were performed using the fully automated Ventana Discovery XT (Roche Diagnostics). Kidney casts were quantified manually using at least 5 different fields at 10× magnification per sample (n = 5 mice per group). The person quantifying the casts was blinded to the genotype. Cleaved caspase-3 activity was assessed by quantifying the cleaved caspase-3 staining area relative to the total field area in 5 microscopy slides at 10× magnification per mouse (n = 5 mice per group) with a semi-automated image analysis of grayscale thresholded images using ImageJ software (NIH).

2.8. Metabolite analyses in urine

Mice urine samples were randomized before proceeding with the sample preparation. Urine (20 μL) was added to 40 μL of PBS buffer (0.2 M phosphate buffer saline pH 7.40 with 0.2 g/L TSP (3-(trimethylsilyl)-2,2′,3,3′-tetradeuteropropionic acid sodium salt) and 0.5 g/L sodium azide in D_2O). The samples were homogenized and centrifuged and 55 μL were transferred into 1.7 mm NMR tubes. NMR spectral acquisition was performed using a Bruker Avance II NMR spectrometer equipped with a 600 MHz magnet Ultrashield Plus and a 1.7 mm probe TXI 1H—^{13}C/D Z-GRD NMR. The temperature was fixed to 300 K for all the NMR measurements. The following ^{1}H NMR experiments were conducted for each sample: ^{1}H NOESY-1D and ^{1}H CPMG-1D (noesygppr1d and cpmgpr1d; a 90° pulse was applied with a relaxation

delay of 4 s and an acquisition time of 2.7 s; the 90° pulse and the pre-saturation power was adjusted automatically for each sample using the pulsecal algorithm; receiver gain 32; spectral width 20 ppm; 65 k time domain; and 256 scans with 4 initial dummy scans, leading to a total of 29 min per experiment). The transmitter frequency offset was manually optimized on the first sample for optimum pre-saturation of the water signal. The spectra were processed using the automated program apk0.noe, which includes Fourier transformation with exponential multiplication, zero-order phase correction, baseline correction, and calibration of the chemical shift axis to TSP = 0 ppm. The NMR spectral acquisition and pre-processing were performed under the control of TopSpin 3.2 (Bruker BioSpin), and the automated submission of a sequence of samples was performed using ICON-NMR (Bruker BioSpin). The BBIOREFFCODE database (Bruker BioSpin), 2D COSY NMR experiments, and literature information enabled NMR signal assignment into metabolite names. In particular, the NAD^+-related metabolites N-methyl-2-pyridone-5-carboxamide (Me2PY) and N-methyl-4-pyridone-5-carboxamide (Me4PY) were previously identified in mice [29] and confirmed by 2D NMR. To overcome the natural dilution effect of the urine samples, the relative quantification of the individual metabolites was performed using the integral intensities of the corresponding spectral regions normalized to the total spectral area (AMIX software, Bruker BioSpin).

2.9. Statistical analyses

Statistical analyses were performed with GraphPad Prism version 7.02 for Windows (La Jolla, CA, USA). Differences between two groups were analyzed using Student's two-tailed t-test. Two-way ANOVA analysis was used when comparing more groups by applying Tukey's post-hoc test. Group variances were similar in all the cases. Unless otherwise specified, all the data are expressed as mean ± S.E.M.

3. RESULTS

3.1. NRH is a potent NAD^+ precursor in cultured cells

NRH is a reduced form of NR (Figure 1A) whose chemical synthesis was recently described [30]. When the AML12 hepatocytes were treated with NRH, the ability of NRH to increase intracellular NAD^+ was vastly superior to that of NR. The dose-response experiments revealed that NRH could significantly increase NAD^+ levels at a concentration of 10 μM (Figure 1B). Even at such a relatively low dose, NRH achieved similar increases in intracellular NAD^+ levels to those reached with NR at 50-fold higher concentrations (Figure 1B). NRH achieved maximal effects on NAD^+ synthesis at approximately 0.5 mM, increasing the intracellular NAD^+ levels by more than 10-fold (Figure 1B). The NRH actions were also extremely fast, as significant increases in NAD^+ levels were observed within 5 min after NRH treatment (Figure 1C). The

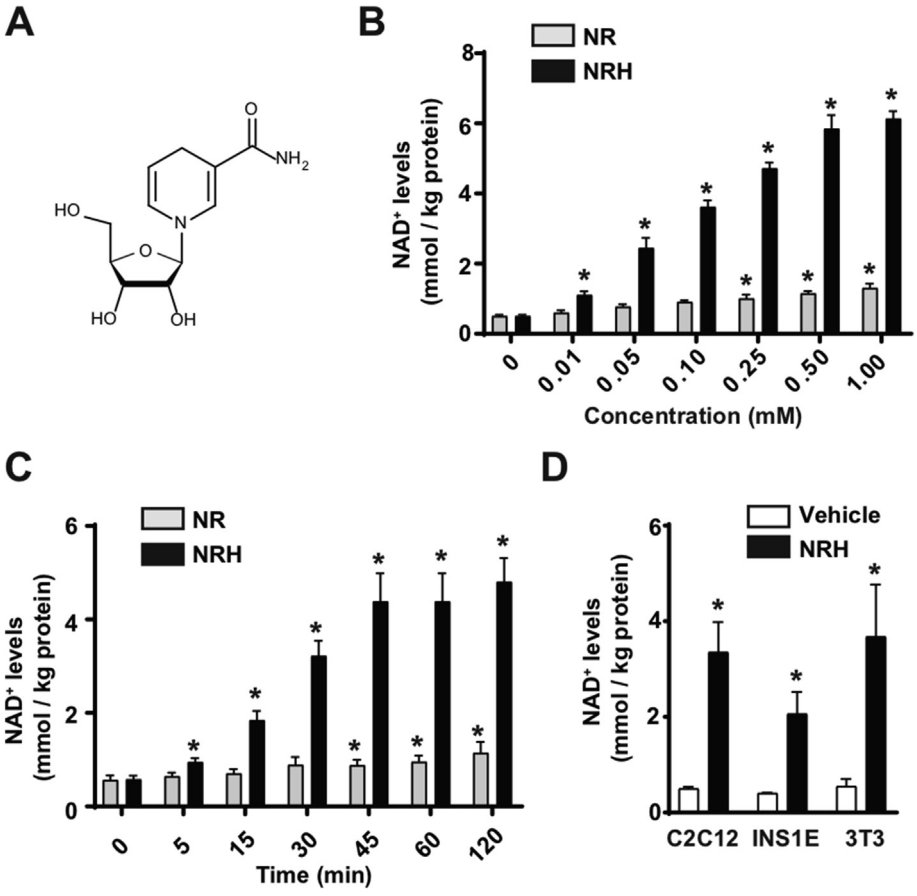

Figure 1: NRH is a potent NAD^+ precursor in mammalian cells. **(A)** Chemical structure of NRH. **(B)** AML12 cells were treated with different doses of NR or NRH and 1 h later acidic extracts were obtained to measure NAD^+ levels. * indicates statistical difference at $p < 0.05$ vs the respective 0 mM group. **(C)** AML12 cells were treated with 0.5 mM NR or NRH for the times indicated. Acidic extracts were obtained to measure NAD^+ levels. * indicates statistical difference at $p < 0.05$ vs the respective t=0 group. **(D)** C2C12 myotubes, INS1E cells, or 3T3 fibroblasts were treated with either PBS (as a vehicle) or NRH (0.5 mM) for 1 h prior to the evaluation of intracellular NAD^+ levels. * indicates statistical difference at $p < 0.05$ vs the vehicle-treated group. All the values in the figure are expressed as mean+/-SEM of n = 3–5 independent experiments.

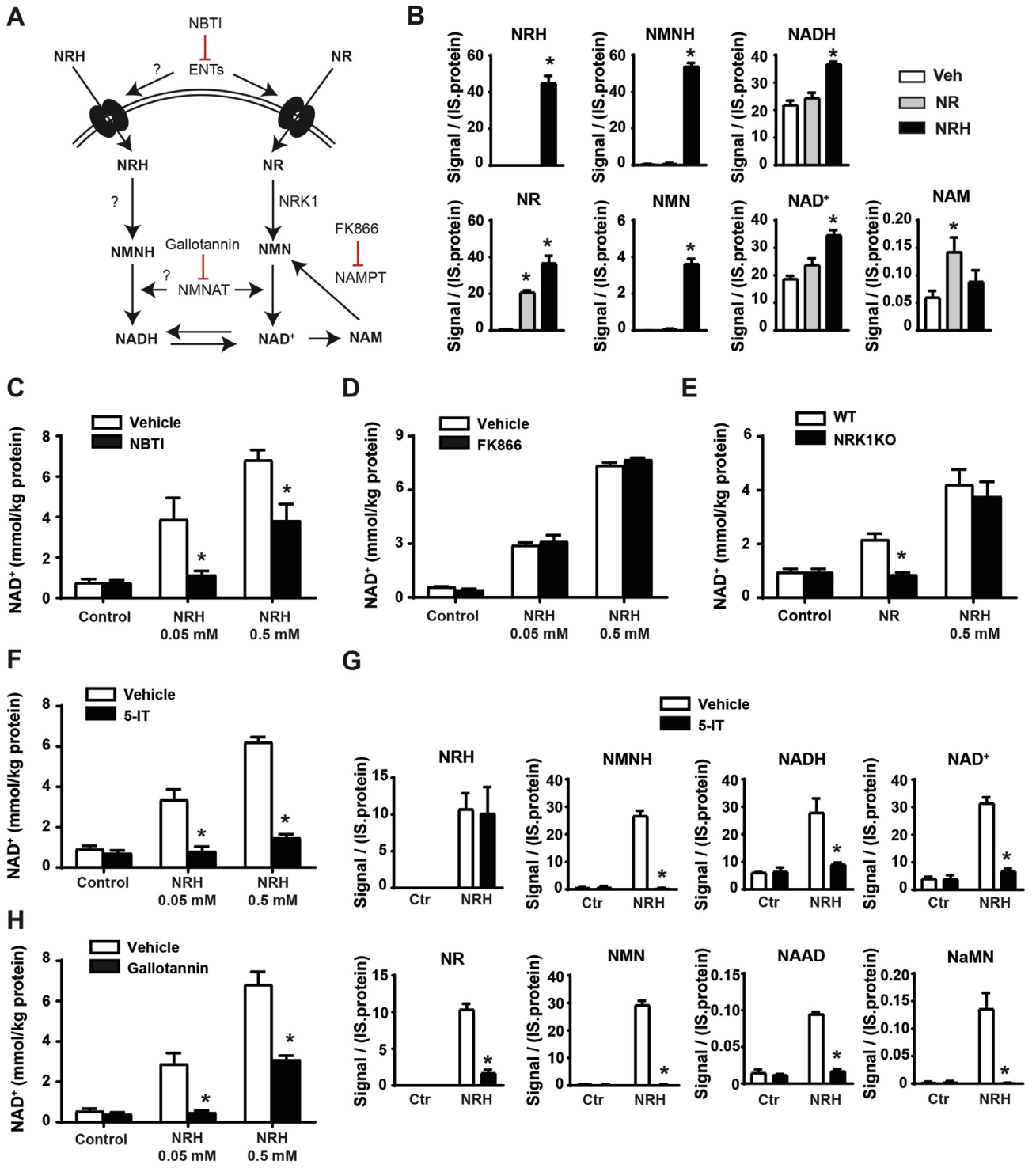

Figure 2: NRH utilization in mammalian cells. **(A)** Scheme of the proposed hypothesis for NHR cellular utilization as a NAD^+ precursor. **(B)** AML12 cells were treated for 5 min with either PBS (as vehicle), NR (0.5 mM), or NRH (0.5 mM). The cells were immediately frozen and used for NAD^+ metabolomic analyses by mass spectrometry. All the results are expressed as intensity of the signal corrected by internal standard (IS) and protein **(C)** AML12 cells were treated with nitrobenzylthioinosine (NBTI) (10 μM) for 1 h prior to NRH treatment at the doses indicated. Then, 1 h later, acidic extracts were obtained to measure NAD^+ levels. **(D)** AML12 cells were treated with FK866 (2 μM) for 1 h prior to NRH treatment at the doses indicated. Then, 1 h later, acidic extracts were obtained to measure NAD^+ levels. **(E)** Primary hepatocytes from either wild-type or NRK1 KO mice were obtained and then treated for 1 h with NRH at the doses indicated. Then, 1 h later, acidic extracts were obtained to measure NAD^+ levels. **(F)** AML12 cells were treated with an adenosine kinase inhibitor (5-IT; 1 μM) for 1 h prior to NRH treatment at the doses indicated. Then, 1 h later, acidic extracts were obtained to measure NAD^+ levels. **(G)** AML12 cells were treated with 5-IT for 1 h prior to NRH treatment (0.05 mM). Then, 5 min later, the cells were snap frozen and processed for NAD^+ metabolomics analyses. All the results are expressed as intensity of the signal, corrected by internal standard (IS) and protein. **(H)** AML12 cells were treated with gallotannin (100 μM) for 1 h prior to NRH treatment at the doses indicated. Then, 1 h later, acidic extracts were obtained to measure NAD^+ levels. All the values in the figure are expressed as mean+/-SEM of 3 independent experiments. * indicates statistical difference at $p < 0.05$ vs the respective vehicle-treated group.

peak levels of NAD^+ were achieved between 45 min and 1 h after treatment (Figure 1C), which also occurred with NR.

NRH treatment highly elevated NAD^+ levels in the C2C12 myotubes, INS1E β-cells, and 3T3 fibroblasts (Figure 1D), supporting the concept that NRH can act as a potent NAD+ precursor in different cell types.

3.2. Deconstructing NRH-induced NAD^+ synthesis

Based on the structural similarity between NRH and NR, we speculated that NRH would follow a very similar metabolism to that of NR to be transformed into NAD^+, but composed of reduced intermediates. This means a path in which NRH would be converted to NMNH, then to NADH, and finally oxidized into NAD^+ (Figure 2A). Accordingly, NRH and NMNH were detected intracellularly 5 min after NRH treatment (Figure 2B). Interestingly, NRH treatment also led to an increase in intracellular NR and NMN, greater than that triggered by NR itself (Figure 2B), opening the possibility that NRH could synthesize NAD^+ by being oxidized to NR using the canonical NRK/NMNAT path.

To understand the exact path by which NRH synthesizes NAD^+, we initially evaluated whether NRH, as NR [21], could be transported into the cell by equilibrative nucleoside transporters (ENTs). Confirming this possibility, NRH largely lost its capacity as an extracellular NAD^+ precursor in the presence of an agent blocking ENT-mediated transport, such as S-(4-nitrobenzyl)-6-thioinosine (NBTI) (Figure 2C). Nevertheless, when the maximal NRH concentrations were used, a substantial increase in NAD^+ remained even after ENT blockage (Figure 2C), suggesting that NRH might be able to enter the cells through alternative low-affinity transporters or that at high doses, NRH can partially override the binding of NBTI to ENTs.

As expected from its chemical structure, the action of NRH was also NAMPT independent (Figure 2D), based on experiments using FK866, an NAMPT inhibitor that completely prevented NAD^+ synthesis from NAM (Supplementary Fig. 1A). If NRH led to NAD^+ synthesis via the formation of NMNH, this hypothetical path would require the phosphorylation of NRH into NMNH. Given the essential and rate-limiting role of NRK1 in NR phosphorylation, we wondered whether the ability of NRH to boost NAD^+ levels was NRK1 dependent. To answer this question, we evaluated NRH action in the primary hepatocytes from either the control or NRK1 knockout (NRK1KO) mice. While after 1 h of treatment, NR failed to increase NAD^+ levels in the NRK1KO-derived primary hepatocytes, NRH action was not affected by NRK1 deficiency (Figure 2E). These results indicate that NRH action is NRK1 independent. Further, they rule out the possibility that NRH-induced NAD^+ synthesis is driven by NRH oxidation into NR.

Considering the molecular structure of NRH, we reasoned that an alternative nucleoside kinase could be responsible for the phosphorylation of NRH. Confirming this expectation, the adenosine kinase (AK) inhibitor 5-iodotubercidin (5-IT) fully ablated the action of NRH (Figure 2F). The critical role of AK in NRH-mediated NAD^+ synthesis was confirmed using a second structurally different AK inhibitor, ABT-702 (Supplementary Fig. 1B). Metabolomic analyses further confirmed that upon inhibition of AK, the generation of NMNH, NADH, and NAD^+ was fully blunted, even if NRH was effectively entering the cell (Figure 2G). Interestingly, 5-IT treatment also prevented the formation of NR and NMN after NRH treatment (Figure 2G). This indicates that the occurrence of NR after NRH treatment cannot be attributed simply to direct NRH intracellular oxidation to NR. As a whole, these experiments depict adenosine kinase as the enzymatic activity catalyzing the conversion of NRH into NMNH, initiating the transformation into NAD^+.

As a follow-up step, NMNAT enzymes could catalyze the transition from NMNH to NADH. Accordingly, the use of gallotannin as a NMNAT inhibitor largely compromised the NAD^+ levels after NRH treatment (Figure 2H). However, part of the NRH action remained after gallotannin treatment when NRH was used at maximal doses. However, the NRH action was totally blocked by gallotannin at submaximal doses, suggesting that the remaining effect at 0.5 mM could be attributed to the incomplete inhibition of NMNAT activity by gallotannin. Given that the concentrations of the different inhibitors in these experiments were based on previous studies using other cultured cell lines, we also cannot fully rule out that the optimal timings/doses for their effectiveness in AML12 might be different. Nevertheless, and as a whole, these results suggest that adenosine kinase and NMNATs constitute the path by which NRH leads to NAD^+ synthesis via NADH.

3.3. NRH is an orally bioavailable NAD^+ precursor in mice

Extracellular NR degradation to NAM could constitute a limitation for its pharmacological efficacy. To evaluate whether NRH was also susceptible to degradation to NAM, we spiked NRH or NR in isolated mouse plasma. After 2 h of incubation at 37 °C, the NR levels decayed in plasma, parallel to an increase in NAM (Figure 3A). In contrast, NAM was not generated from NRH, as its levels remained stable during the 2-hour test (Figure 3A). We also tested the stability of NRH in other matrixes. Given our previous experiments with cultured cells, we verified that NRH did not degrade to NAM in FBS-supplemented media, as occurs with NR (Supplementary Fig. 2A). Finally, we also certified NRH's stability in water (pH = 7, at room temperature) for 48 h (Supplementary Fig. 2B).

These results prompted us to test whether NRH could act as an effective NAD^+ precursor *in vivo*. For this, we first intraperitoneally (IP) injected mice with either NR or NRH at 250 mg/kg and 500 mg/kg. After 1 h, both compounds increased hepatic NAD^+ levels in a dose-dependent manner, yet NRH led to markedly higher effects than NR at all doses (Figure 3B). NRH also showed a superior capacity to trigger NAD^+ synthesis in muscle, as both the 250 mg/kg and 500 mg/kg doses increased intramuscular NAD^+ levels 1 h after administration, while NR achieved significant increases only at 500 mg/kg (Figure 3B). NRH and NR largely increased renal NAD^+ levels, albeit NRH was more potent at 250 mg/kg. Notably, NRH's effects were not significantly superior to those of NR at 500 mg/kg, most likely because the kidney has a high NRK1 expression and steeply responds to NR after IP injection (Figure 3B and [20]). These results highlight that NRH is a very effective NAD^+ precursor *in vivo* after intraperitoneal injection.

As expected based on our previous research [20], NAM levels were highly increased in circulation upon NR administration at 250 mg/kg, while only a very mild increase in circulating NAM was observed with NRH at a similar dose (Figure 3C). Importantly, NRH was detectable in circulation after IP injection (Figure 3C). Strikingly, NR was also detectable in circulation after NRH treatment at much higher levels than those detected after NR injection itself (Figure 3C). Very similar outcomes were observed when the compounds were injected at 500 mg/kg (Supplementary Fig. 2C). Given that NRH incubation in isolated plasma did not lead to NR production (Figure 3A), the appearance of NR might be consequent to intracellular production and release to circulation. Similarly, the residual appearance of NAM after NRH treatment might be explained by the degradation of released NR or by the release of intracellular NAM as a product of NAD^+ degradation, as NRH did not significantly alter NAM levels when incubated in isolated plasma (Figure 3A).

Oral administration of NRH (500 mg/kg) led to very similar results to those observed after IP administration. First, NRH had a more potent effect on hepatic NAD^+ levels than NR (Figure 3D). NRH was detectable in plasma 1 h after oral administration (Figure 3E). In contrast, NR

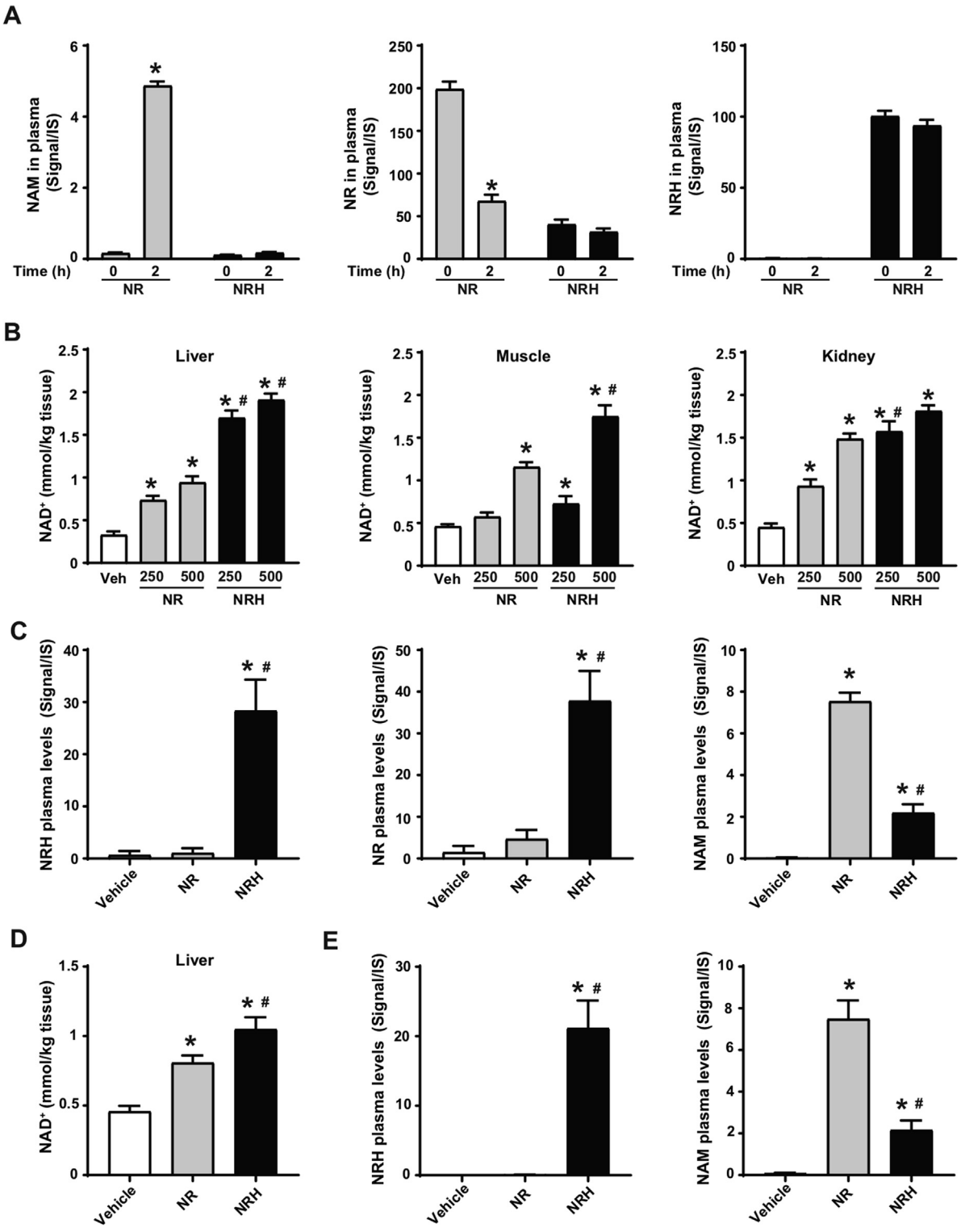

Figure 3: NRH is orally bioavailable and does not degrade in plasma. **(A)** Mouse plasma was isolated and then spiked with either NR (0.5 mM) or NRH (0.5 mM). Samples were then snap frozen immediately after spiking with the compound or after 2 h of incubation at 37 °C. NAM, NR, and NRH were measured by LC-MS. The results are presented as the peak signal corrected by internal standard (IS). * indicates statistical difference vs the respective t = 0 group at $p < 0.05$. **(B)** Eight-week-old C57Bl/6NTac mice were intraperitoneally injected with either saline (as vehicle), NR or NRH at either 250 or 500 mg/kg. One hour later, tissue samples were collected and immediately frozen. Acidic extracts were obtained from the liver, muscle, and kidney to measure NAD^+ levels. **(C)** Evaluation of NAM, NR, and NRH levels in the mice plasma 1 h after the intraperitoneal injection of saline (as a vehicle) or 250 mg/kg of NR or NRH. **(D–E)** Eight-week-old C57Bl/6NTac mice were orally gavaged with either saline (as a vehicle), NR (500 mg/kg), or NRH (500 mg/kg). After 1 h, hepatic NAD^+ levels (D) and circulating levels of NRH and NAM (E) were evaluated as in (C). All the results are expressed as mean+/-SEM of 3 independent experiments (A) or n = 5 mice per group (B–E). In panels B–E, * indicates statistical difference at $p < 0.05$ vs the saline-treated mice. # indicates statistical difference at $p < 0.05$ vs the NR-treated mice at the respective dose.

levels were undetectable at 1 h after NR administration (Supplementary Fig. 2D). As expected, NR treatment led to large increases in circulating NAM, which were ~4-fold higher than those observed after NRH treatment (Figure 3E). Quantification measurements revealed that after oral gavage, NRH concentration in plasma reached 11.2 ± 1.7 μmol/L, which, as described in Figure 1, was enough to drive NAD^+ synthesis in the cultured cells. These results illustrate that NRH is a potent orally bioavailable NAD^+ precursor that overcomes direct degradation to NAM in plasma.

3.4. NRH protects against cisplatin-induced acute kidney injury

NAD^+ precursor supplementation has recently emerged as a valid strategy to treat or alleviate features of metabolic and age-related diseases in pre-clinical models [1]. In particular, recent efforts indicate that supplementation with NMN or NAM can be protective against acute kidney injury (AKI) in mice [15,31]. Further, a recent study demonstrated a critical role of NAD^+ maintenance in human AKI [32]. We hence chose AKI as a disease model to evaluate the potential therapeutic actions of NRH. For this purpose, we injected 8-week-old mice with either saline (as a control) or cisplatin (20 mg/kg). The mice were then repeatedly injected with either PBS (as vehicle) or NRH (250 mg/kg) at 0, 24, 48, and 72 h after cisplatin injection. The use of NRH at 250 mg/kg was chosen in light of our previous results showing that it achieves maximal effects on kidney NAD^+ synthesis 1 h after administration (Figure 3B). The mice were euthanized 4 h after the last NRH injection. As displayed in Figure 4A, cisplatin treatment led to a decrease in kidney NAD^+ and NADH levels in parallel to an increase in NAM and Me-NAM levels. This was also reflected in the levels of methylated-oxidized NAM metabolites in the urine, namely Me2PY and Me4PY (Supplementary Fig. 3A). NRH supplementation prevented a decrease in the renal NAD^+ and NADH levels induced by cisplatin (Figure 4A). We did not observe higher NAD^+ levels in the kidney of the control mice 4 h after NRH supplementation. This could be due to a high NAD^+ turnover rate in the kidney, as increased NAD^+ was observed in shorter time frames (Figure 3B). Interestingly, NRH further increased Me-NAM levels in the kidney and Me2PY and Me4PY levels in the urine (Supplementary Fig. 3A). These results indicate that cisplatin sparked NAD^+ consumption and NRH effectively sustained NAD^+ levels upon cisplatin treatment.

The decrease in NAD^+ levels triggered by cisplatin could be related to its genotoxic activity, leading to enhanced DNA damage and PARP activity. Accordingly, cisplatin increased PARP1 levels and PARP activity in our intervention (Figure 4B and Supplementary Fig. 3B). We next hypothesized that the NAD^+ crisis occurring after cisplatin treatment could limit PARP activity, leading to unresolved DNA damage and prompting kidney failure. If this was true, the recovery of NAD^+ levels with NRH should lead to enhanced PARP activity. In line with that, NRH treatment markedly increased PARP activity in the cisplatin-treated mice in the absence of changes in PARP1 levels (Figure 4B and Supplementary Fig. 3B). Altogether, these results are consistent with a scenario in which cisplatin-triggered PARP activity increases the rate of NAD^+ degradation to NAM, leading to a drop in the total NAD^+ levels that ultimately limits PARP activity itself. In this setting, NRH helped sustain NAD^+ levels and PARP activity.

We next wondered whether the ability of NRH to sustain NAD^+ levels and PARP activity upon cisplatin treatment also translated into protection against kidney failure. Supporting this possibility, NRH injections alleviated increases in the blood urea nitrogen (BUN) induced by cisplatin (Figure 4C). Concomitantly, the urea levels in the urine were higher upon NRH treatment (Figure 4D), further suggesting better renal function. At the histological level, NRH treatment *per se* did not lead to any major ultrastructural change in the kidney (Figure 4E). Cisplatin treatment markedly altered the kidney structure, including increased tubular necrosis, glomeruli dilatation, inflammation, and cast formation. These pathological features were largely absent when cisplatin treatment was combined with NRH (Figure 4E), as exemplified by the close to total prevention against the formation of kidney casts (Figure 4F). To further verify this point, we next analyzed the mRNA expression levels of markers for glomerular dysfunction (fibronectin), ER stress (BIP/Gpr78), or apoptosis (BAX), all of which are characteristic of cisplatin-induced kidney damage [33–35]. NRH blunted the increase in fibronectin and BIP expression induced by cisplatin treatment, while also partially reducing cisplatin-induced BAX mRNA levels (Figure 4G). These improvements could be due to the ability of NRH to prevent the increase in TGF-β1, a key triggering agent for renal apoptosis and fibrogenesis after cisplatin treatment [36]. In line with these results, NRH largely prevented the increase in cleaved caspase-3 observed after cisplatin treatment, as demonstrated through histology (Supplementary Fig. 3C).

4. DISCUSSION

To date, it has been generally considered that 5 molecules can act as direct extracellular NAD^+ precursors: tryptophan, NA, NAM, nicotinic acid riboside (NaR), and NR [1]. Here, we report a new NAD^+ precursor, NRH. The reduction of the NR molecule to NRH confers it not only a much stronger capacity to increase intracellular NAD^+ levels but also different selectivity in terms of its cellular use.

In cultured cells, NRH acted as an extremely potent NAD^+ inducer, increasing intracellular NAD^+ between 5- and 10-fold above basal levels in different cell lines. During the writing of this article, another study reported similar findings on the ability of NRH to enhance NAD^+ levels [37]. However, the metabolic path used by NRH was not identified in this report. Our study answers this question and demonstrates that NRH requires phosphorylation by AK for its conversion to NMNH and subsequently to NADH and NAD^+. In agreement with Yang et al. [37], we also observed a prominent increase in intracellular NR and NMN after NRH administration. However, this increase was completely prevented upon inhibition of AK activity, suggesting that the increase in NR and NMN is secondary to the increase in NAD^+ promoted by NRH and not simply due to NRH oxidation to NR inside the cell. Furthermore, because the action of NRH on NAD^+ is intact in NRK1 KO hepatocytes, this increase in NR is unlikely to drive NAD^+ production by NRH. Therefore, how can NRH drive an increase in NR? Evidence suggests that upon high NAD^+ synthesis rates from one path, other canonical paths for NAD^+ synthesis might be reversed. This concept was initially proposed based on the observation that NR supplementation led to a peak in NAAD production [22]. The use of stable isotope tracers certified that this NAAD was derived directly from NR and not from its canonical precursor, NA [20]. Hence, it was proposed that either NAD^+ or NMN could be deamidated to NAAD or NaMN, respectively. In agreement, our results indicate that the intracellular metabolism of NRH also increased NAAD and NaMN levels. With respect to NR, evidence in yeast indicates that NR can be produced from NMN and released to the medium, acting as a NAD^+ precursor on neighboring cells [38]. Kulikova et al. recently demonstrated that, to some extent, mammalian cells might also be capable of performing the same reaction [39]. Our results support this possibility and suggest that NRH must initially be converted to NMNH. The high flux of NAD^+ production attained through this path will reverse the canonical reactions for NAD^+ synthesis from NR. The identity of the specific enzymes

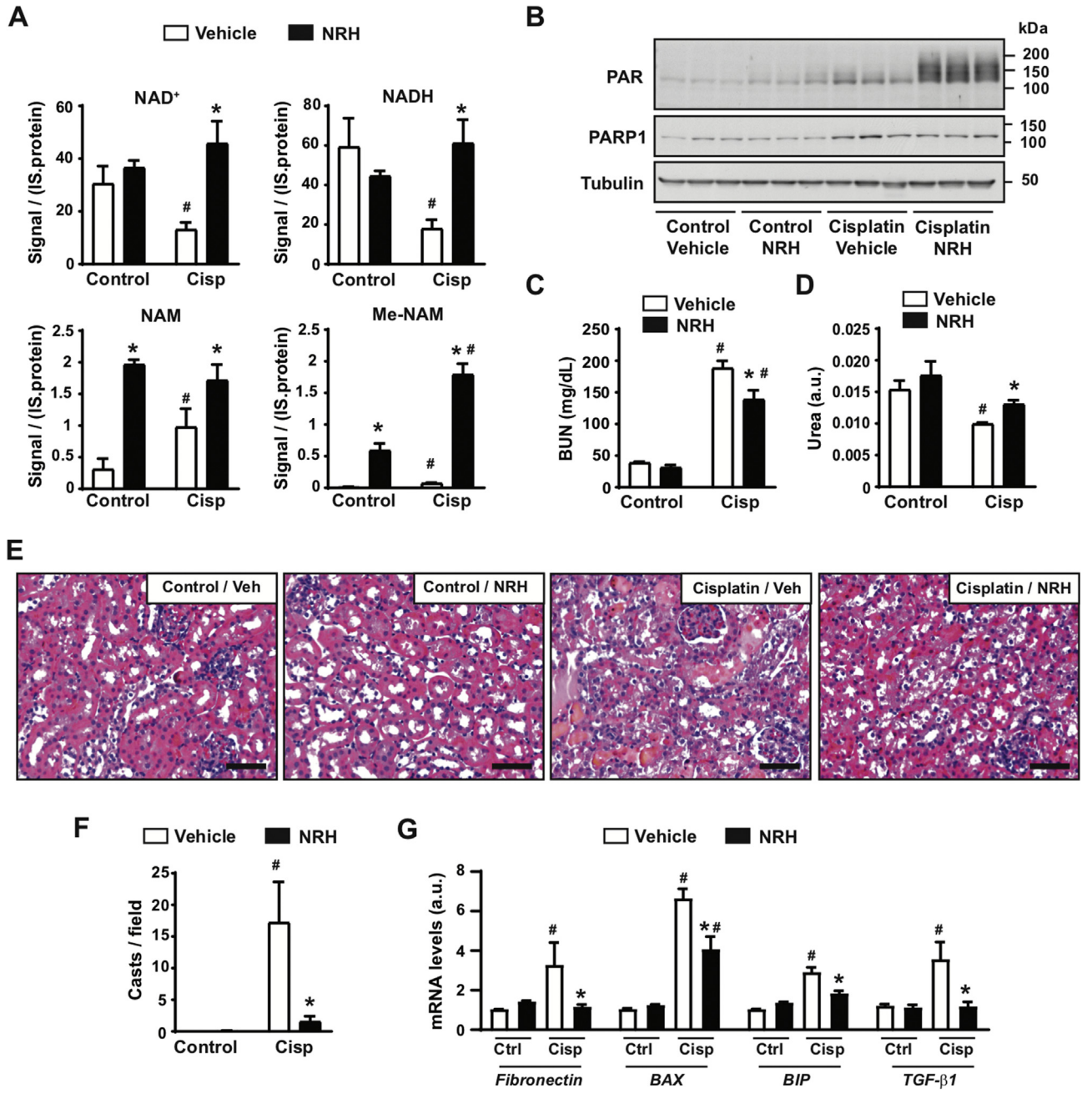

Figure 4: NRH protects against cisplatin-induced acute kidney injury. Eight-week-old C57Bl/6NTac mice were intraperitoneally injected with either saline (control group) or cisplatin (20 mg/kg). Simultaneously, the mice were intraperitoneally injected or not injected with PBS (vehicle) or NRH (250 mg/kg). PBS or NRH were then injected at 24, 48, and 72 h after the initiation of the experiment, immediately after collecting urine. The mice were sacrificed 4 h after the last injection, and urine, blood, and kidneys were collected. **(A)** NAD^+ metabolites levels in the kidney were measured by mass spectrometry. The results are expressed as the peak signal corrected by internal standard (IS) and protein. **(B)** Total kidney protein extracts were used to measure poly-ADPribosylation levels and PARP1. Tubulin was used as a loading control. Quantifications for these blots can be found in Supplementary Fig. 3B. **(C)** Blood urea nitrogen levels in the mice plasma. **(D)** Urea levels in urine 24 h after the initiation of the experiment. **(E)** H&E staining of the kidney. Bar length: 100 μM. **(F)** Quantification of kidney casts from histology images. **(G)** Total mRNA was extracted from the kidney to evaluate the markers indicated by RT-qPCR. All the values are expressed as mean+/-SEM of $n = 4$ mice per group. * indicates statistical difference at $p < 0.05$ between the respective NRH and vehicle-injected mice. # indicates statistical difference at $p < 0.05$ between the respective cisplatin and control groups.

accounting for NMN production from NAD^+ or NR production from NMN will need to be defined in future studies. Another limitation of our study is that the relative metabolite concentrations obtained by metabolomic analyses of NAD^+ metabolic intermediates, while informative and efficient in the comparison between treatments, do not fully describe NAD^+ turnover and precursor contribution. NAD^+ biosynthesis is ramified, and most of the involved metabolic reactions are reversible. Future studies using complementary strategies such as absolute quantitation of intermediates or tracer studies will likely lead to a more precise estimate of the contribution and, therefore, the physiological significance of each of the different metabolites to the overall NAD^+ metabolome after NRH treatment.

NRH proved to be an efficient NAD^+ precursor in mice, displaying higher effects than NR in the liver and muscle after intraperitoneal injection. At least two independent elements could contribute to this. First, it could be speculated that AK enzymatic properties allow for a faster conversion of NRH into NMNH than NRK1 does to convert NR into NMN. A second possibility could be that, in contrast to NR, NRH is not degraded to NAM in plasma. This would provide a greater advantage for NAD^+ synthesis, as extracellular NAM is a weak NAD^+ precursor in multiple cells and tissues [20]. Regarding NR degradation to NAM, we previously reported that NR quickly disappears from the bloodstream, and is almost undetectable 1 h after intraperitoneal administration at 500 mg/kg [20]. Nevertheless, evidence indicates that NR is directly used as a NAD^+ precursor during this time. First, the increase in NAD^+ levels observed in multiple tissues after intraperitoneal administration of NR was largely compromised in the NRK1-deficient mice [20]. Second, elegant tracer experiments demonstrated that after oral intake, NR was utilized as such by the liver, while it predominantly reached the peripheral tissues as its degradation product, NAM [26]. Third, the oral administration of NR improved functional deficits and restored muscle mass in muscle-specific Nampt knockout mice [40]. Altogether, these results demonstrate that NR effectively reaches tissues after intraperitoneal or oral administration, but its circulating levels, and, hence, direct action as a NAD^+ precursor, are quickly curtailed by degradation to NAM. Our results suggest that NRH could bypass this limitation, as it is not susceptible to direct degradation in plasma. Supporting this point, NRH was detectable in circulation after intraperitoneal injection or oral intake. Interestingly, NR was detected in circulation after NRH administration at much higher levels than those observed after direct NR administration. Several observations suggest that NR's appearance after NRH treatment is unlikely to occur through a nonenzymatic tilting of the redox balance between NRH and NR. First, the experiments in isolated plasma demonstrate that NRH does not lead to significant NR production over time. The intraperitoneal NR injections in mice demonstrate that NR has a short life in circulation, as no NR is detectable 1 h after administration. Therefore, an initial redox equilibration between NRH and NR cannot explain a higher presence of NR in circulation in the NRH vs the NR injected group 1 h after administration. Second, our experiments in cultured cells indicate that NR is produced intracellularly as a product of NRH metabolism. Hence, we speculate that NR in circulation detected 1 h after NRH administration could be consequent to an outward flux of NR via ENT transporters. This could occur if the intracellular NR concentration was higher than that in circulation, especially if NR accumulates in cells with limited NRK activity.

Our results of cisplatin-induced AKI also suggest a therapeutic potential for NRH. Previous observations indicate a particularly high expression of NAD^+ biosynthetic enzymes in the kidney [20,41], suggesting high NAD^+ turnover. The need for high NAD^+ synthesis capacity might be a protective strategy, as defects in renal NAD^+ are causally associated with kidney injury [31,32]. In line with this, the dietary supplementation with NAD^+-boosting compounds, such as NMN [15] or α-amino-β-carboxymuconate-ε-semialdehyde decarboxylase (ACMSD) inhibitors [41], conferred protection against ischemic and chemotoxicity models of AKI. Our results support these previous observations and establish NRH as a new molecule to counteract the detrimental effects of cisplatin on renal function. Furthermore, the metabolomic analyses on our samples support a model in which NRH-induced NAD^+ synthesis allows sustaining NAD^+ levels and the catalytic rates of PARP enzymes, which are critical to recover from cisplatin-induced cellular damage, ultimately leading to the ultrastructural and functional protection of the kidney. It will be interesting to evaluate in future experiments whether the superior capacity of NRH to trigger NAD^+ synthesis translates into higher therapeutic efficacy when compared with NR, NMN, or other NAD^+ precursors at similar doses.

In conclusion, this study expands the current understanding of NAD^+ metabolism by revealing a new precursor and pathway for NAD^+ biosynthesis. We further demonstrate that NRH is orally bioavailable and that it could constitute a valid alternative for therapies based on enhancing NAD^+ levels. One key question for follow-up studies will be to identify the clinical significance of NRH and its physiological role. One could speculate that NRH could be a product of extracellular NADH degradation, as NR can be a product of extracellular NAD^+ degradation, for example, when these metabolites are released upon the death of neighboring cells.

AUTHOR CONTRIBUTIONS

JGG, RZP, RHH, MEM, SM, and CC conceived the project and experiments. JGG, MJ, and AC performed cell culture experiments. JGG, JLSG, and CC experiments in animal models. MPG, SB, and SM developed and performed all metabolomic analyses. MVM and MEM synthesized NRH. JGG and CC wrote the manuscript, and all authors contributed to its editing.

ACKNOWLEDGMENTS

The authors thank Jessica Dessimoz at the Histology Platform from the Ecole Polytechnique Fédérale de Lausanne (EPFL) for technical and scientific support in the performance of histology analyses. This research was funded by Nestlé Research Ltd. CC was also funded by the EU Marie Sklodowska-Curie ITN-ChroMe (H2020-MSCA ITN-2015-ChroMe-project number 675610). RZP was supported by a post-doctoral grant from the European Union's Horizon 2020 research and innovation program under the Marie Sklodowska-Curie grant agreement number 840110 and from Fundación Séneca - Agencia de Ciencia y Tecnología de la Región de Murcia. We also thank NIH (NCCIH R21 grant AT009908-01) for financial support to MEM and MVM.

CONFLICTS OF INTEREST

JGG, MJ, MPG, AC, SB, JLSG, SM, and CC are employees of the Nestlé Institute of Health Sciences, which is part of Nestlé Research Ltd.

APPENDIX A. SUPPLEMENTARY DATA

Supplementary data to this article can be found online at https://doi.org/10.1016/j.molmet.2019.09.013.

REFERENCES

[1] Canto, C., Menzies, K.J., Auwerx, J., 2015. NAD^+ metabolism and the control of energy homeostasis: a balancing act between mitochondria and the nucleus. Cell Metabolism 22(1):31—53.

[2] Imai, S., Armstrong, C.M., Kaeberlein, M., Guarente, L., 2000. Transcriptional silencing and longevity protein Sir2 is an NAD-dependent histone deacetylase. Nature 403(6771):795—800.

[3] Chambon, P., Weill, J.D., Mandel, P., 1963. Nicotinamide mononucleotide activation of new DNA-dependent polyadenylic acid synthesizing nuclear enzyme. Biochemical and Biophysical Research Communications, 1139—1143.

[4] Lee, H.C., Aarhus, R., 1991. ADP-ribosyl cyclase: an enzyme that cyclizes NAD+ into a calcium-mobilizing metabolite. Cell Regulation 2(3):203—209.

[5] Bieganowski, P., Brenner, C., 2004. Discoveries of nicotinamide riboside as a nutrient and conserved NRK genes establish a Preiss-Handler independent route to NAD+ in fungi and humans. Cell 117(4):495–502.

[6] Belenky, P., Bogan, K.L., Brenner, C., 2007. NAD+ metabolism in health and disease. Trends in Biochemical Sciences 32(1):12–19.

[7] Benyo, Z., Gille, A., Kero, J., Csiky, M., Suchankova, M.C., Nusing, R.M., et al., 2005. GPR109A (PUMA-G/HM74A) mediates nicotinic acid-induced flushing. Journal of Clinical Investigation 115(12):3634–3640.

[8] Soga, T., Kamohara, M., Takasaki, J., Matsumoto, S., Saito, T., Ohishi, T., et al., 2003. Molecular identification of nicotinic acid receptor. Biochemical and Biophysical Research Communications 303(1):364–369.

[9] Tunaru, S., Kero, J., Schaub, A., Wufka, C., Blaukat, A., Pfeffer, K., et al., 2003. PUMA-G and HM74 are receptors for nicotinic acid and mediate its anti-lipolytic effect. Nature Medicine 9(3):352–355.

[10] Wise, A., Foord, S.M., Fraser, N.J., Barnes, A.A., Elshourbagy, N., Eilert, M., et al., 2003. Molecular identification of high and low affinity receptors for nicotinic acid. Journal of Biological Chemistry 278(11):9869–9874.

[11] Canto, C., Houtkooper, R.H., Pirinen, E., Youn, D.Y., Oosterveer, M.H., Cen, Y., et al., 2012. The NAD^+ precursor nicotinamide riboside enhances oxidative metabolism and protects against high-fat diet-induced obesity. Cell Metabolism 15(6):838–847.

[12] Yoshino, J., Mills, K.F., Yoon, M.J., Imai, S., 2011. Nicotinamide mononucleotide, a key NAD^+ intermediate, treats the pathophysiology of diet- and age-induced diabetes in mice. Cell Metabolism 14(4):528–536.

[13] Trammell, S.A., Weidemann, B.J., Chadda, A., Yorek, M.S., Holmes, A., Coppey, L.J., et al., 2016. Nicotinamide riboside opposes type 2 diabetes and neuropathy in mice. Scientific Reports, 626933.

[14] Gariani, K., Menzies, K.J., Ryu, D., Wegner, C.J., Wang, X., Ropelle, E.R., et al., 2016. Eliciting the mitochondrial unfolded protein response by nicotinamide adenine dinucleotide repletion reverses fatty liver disease in mice. Hepatology 63(4):1190–1204.

[15] Guan, Y., Wang, S.R., Huang, X.Z., Xie, Q.H., Xu, Y.Y., Shang, D., et al., 2017. Nicotinamide mononucleotide, an NAD^+ precursor, rescues age-associated susceptibility to AKI in a sirtuin 1-dependent manner. Journal of the American Society of Nephrology 28(8):2337–2352.

[16] Mills, K.F., Yoshida, S., Stein, L.R., Grozio, A., Kubota, S., Sasaki, Y., et al., 2016. Long-term administration of nicotinamide mononucleotide mitigates age-associated physiological decline in mice. Cell Metabolism 24(6):795–806.

[17] Zhang, H., Ryu, D., Wu, Y., Gariani, K., Wang, X., Luan, P., et al., 2016. NAD^+ repletion improves mitochondrial and stem cell function and enhances life span in mice. Science 352(6292):1436–1443.

[18] Belenky, P., Racette, F.G., Bogan, K.L., McClure, J.M., Smith, J.S., Brenner, C., 2007. Nicotinamide riboside promotes Sir2 silencing and extends lifespan via Nrk and Urh1/Pnp1/Meu1 pathways to NAD+. Cell 129(3):473–484.

[19] Mouchiroud, L., Houtkooper, R.H., Moullan, N., Katsyuba, E., Ryu, D., Canto, C., et al., 2013. The NAD^+/Sirtuin pathway modulates longevity through activation of mitochondrial UPR and FOXO signaling. Cell 154(2):430–441.

[20] Ratajczak, J., Joffraud, M., Trammell, S.A., Ras, R., Canela, N., Boutant, M., et al., 2016. NRK1 controls nicotinamide mononucleotide and nicotinamide riboside metabolism in mammalian cells. Nature Communications, 713103.

[21] Nikiforov, A., Dolle, C., Niere, M., Ziegler, M., 2011. Pathways and subcellular compartmentation of NAD biosynthesis in human cells: from entry of extracellular precursors to mitochondrial NAD generation. Journal of Biological Chemistry 286(24):21767–21778.

[22] Trammell, S.A., Schmidt, M.S., Weidemann, B.J., Redpath, P., Jaksch, F., Dellinger, R.W., et al., 2016. Nicotinamide riboside is uniquely and orally bioavailable in mice and humans. Nature Communications, 712948.

[23] Dollerup, O.L., Christensen, B., Svart, M., Schmidt, M.S., Sulek, K., Ringgaard, S., et al., 2018. A randomized placebo-controlled clinical trial of nicotinamide riboside in obese men: safety, insulin-sensitivity, and lipid-mobilizing effects. American Journal of Clinical Nutrition 108(2):343–353.

[24] Martens, C.R., Denman, B.A., Mazzo, M.R., Armstrong, M.L., Reisdorph, N., McQueen, M.B., et al., 2018. Chronic nicotinamide riboside supplementation is well-tolerated and elevates NAD^+ in healthy middle-aged and older adults. Nature Communications 9(1):1286.

[25] Dolopikou, C.F., Kourtzidis, I.A., Margaritelis, N.V., Vrabas, I.S., Koidou, I., Kyparos, A., et al., 2019. Acute nicotinamide riboside supplementation improves redox homeostasis and exercise performance in old individuals: a double-blind cross-over study. European Journal of Nutrition.

[26] Liu, L., Su, X., Quinn 3rd, W.J., Hui, S., Krukenberg, K., Frederick, D.W., et al., 2018. Quantitative analysis of NAD synthesis-breakdown fluxes. Cell Metabolism 27(5):1067–1080 e5.

[27] Berger, F., Lau, C., Dahlmann, M., Ziegler, M., 2005. Subcellular compartmentation and differential catalytic properties of the three human nicotinamide mononucleotide adenylyltransferase isoforms. Journal of Biological Chemistry 280(43):36334–36341.

[28] Ramesh, G., Ranganathan, P., 2014. Mouse models and methods for studying human disease, acute kidney injury (AKI). Methods in Molecular Biology, 1194421–1194436.

[29] Wong, P., Bachki, A., Banerjee, K., Leyland-Jones, B., 2002. Identification of N1-methyl-2-pyridone-5-carboxamide and N1-methyl-4-pyridone-5-carboxamide as components in urine extracts of individuals consuming coffee. Journal of Pharmaceutical and Biomedical Analysis 30(3):773–780.

[30] Makarov, M.V., Migaud, M.E., 2019. Syntheses and chemical properties of beta-nicotinamide riboside and its analogues and derivatives. Beilstein Journal of Organic Chemistry, 15401–15430.

[31] Tran, M.T., Zsengeller, Z.K., Berg, A.H., Khankin, E.V., Bhasin, M.K., Kim, W., et al., 2016. PGC1alpha drives NAD biosynthesis linking oxidative metabolism to renal protection. Nature 531(7595):528–532.

[32] Poyan Mehr, A., Tran, M.T., Ralto, K.M., Leaf, D.E., Washco, V., Messmer, J., et al., 2018. De novo NAD^+ biosynthetic impairment in acute kidney injury in humans. Nature Medicine 24(9):1351–1359.

[33] Ozkok, A., Edelstein, C.L., 2014. Pathophysiology of cisplatin-induced acute kidney injury. BioMed Research International, 2014967826.

[34] Miller, R.P., Tadagavadi, R.K., Ramesh, G., Reeves, W.B., 2010. Mechanisms of cisplatin nephrotoxicity. Toxins (Basel) 2(11):2490–2518.

[35] Mandic, A., Hansson, J., Linder, S., Shoshan, M.C., 2003. Cisplatin induces endoplasmic reticulum stress and nucleus-independent apoptotic signaling. Journal of Biological Chemistry 278(11):9100–9106.

[36] Bottinger, E.P., Bitzer, M., 2002. TGF-beta signaling in renal disease. Journal of the American Society of Nephrology 13(10):2600–2610.

[37] Yang, Y., Mohammed, F.S., Zhang, N., Sauve, A.A., 2019. Dihydronicotinamide riboside is a potent NAD^+ concentration enhancer in vitro and in vivo. Journal of Biological Chemistry.

[38] Bogan, K.L., Evans, C., Belenky, P., Song, P., Burant, C.F., Kennedy, R., et al., 2009. Identification of Isn1 and Sdt1 as glucose- and vitamin-regulated nicotinamide mononucleotide and nicotinic acid mononucleotide [corrected] 5′-nucleotidases responsible for production of nicotinamide riboside and nicotinic acid riboside. Journal of Biological Chemistry 284(50):34861–34869.

[39] Kulikova, V., Shabalin, K., Nerinovski, K., Dolle, C., Niere, M., Yakimov, A., et al., 2015. Generation, release, and uptake of the NAD precursor nicotinic acid riboside by human cells. Journal of Biological Chemistry 290(45):27124–27137.

[40] Frederick, D.W., Loro, E., Liu, L., Davila Jr., A., Chellappa, K., Silverman, I.M., et al., 2016. Loss of NAD homeostasis leads to progressive and reversible degeneration of skeletal muscle. Cell Metabolism 24(2):269–282.

[41] Katsyuba, E., Mottis, A., Zietak, M., De Franco, F., van der Velpen, V., Gariani, K., et al., 2018. De novo NAD^+ synthesis enhances mitochondrial function and improves health. Nature 563(7731):354–359.

